Measurement of the velocity difference by photon correlation spectroscopy: an improved scheme

Theyencheri Narayanan, Cecil Cheung, Penger Tong, Walter I. Goldburg, and Xiao-lun Wu

Homodyne photon correlation spectroscopy is used to measure the velocity difference $\delta\mathbf{v}(l)$ over varying distance l. Different length scales are probed when the magnification factor M and the width S of a slit in the collecting optics are varied. The measured intensity autocorrelation function is found to be of scaling form for different values of M, provided S is kept at a value below the critical width S_c. A new convenient collecting optics is devised to expand the variable range of l up to 2 decades, over which $\delta\mathbf{v}(l)$ can be accurately measured. The new scheme is useful for the study of turbulent and other self-similar flows. © 1997 Optical Society of America

Key words: Photon correlation spectroscopy, spatial coherence, turbulent flow, velocity difference.

1. Introduction

In studies of turbulent flows, one is often interested in measuring the velocity difference $\delta\mathbf{v}(\mathbf{r}) = \mathbf{v}(\mathbf{x}) - \mathbf{v}(\mathbf{x} + \mathbf{r})$ rather than the local velocity $\mathbf{v}(\mathbf{x})$. As was demonstrated many years ago,[1,2] the velocity difference $\delta\mathbf{v}(\mathbf{r})$ is accessible by homodyne photon correlation spectroscopy (PCS). With the PCS technique, small seed particles that follow the local flow of the fluid scatter the light from a laser. A photodetector records the scattered light intensity, which fluctuates because of the motion of the particles. The output signal of the detector is therefore modulated at a frequency equal to the difference in Doppler shifts of all particle pairs in the scattering volume. For each particle pair separated by a distance r (along the beam-propagation direction), this difference is $\mathbf{q} \cdot \delta\mathbf{v}(r)$, where $\mathbf{q}$ is the momentum transfer vector. The magnitude of $\mathbf{q}$ is given by $q = (4\pi n/\lambda)\sin(\theta/2)$, where θ is the scattering angle, n is the refractive index of the fluid, and λ is the wavelength of the incident light. With the homodyne method, one measures the intensity autocorrelation function[3]

$$g(\tau) = \frac{\langle I(t+\tau)I(t)\rangle}{\langle I(t)\rangle^2} = 1 + bG(\tau), \qquad (1)$$

where $I(t)$ is the intensity of the scattered light, b (≤ 1) is an instrumental constant, and $\langle \ldots \rangle$ denotes a time average.

It has been shown that the function $G(\tau)$ in Eq. (1) has the form[4]

$$G(\tau) = \int_0^l \mathrm{d}r h(r) \int_{-\infty}^{\infty} \mathrm{d}\delta v P(\delta v, r)\cos(q\tau\delta v), \qquad (2)$$

where $\delta v(r)$ is the component of $\delta\mathbf{v}(r)$ in the direction of $\mathbf{q}$, and $h(r)\mathrm{d}r = [2(1 - r/l)/l]\mathrm{d}r$ is the number fraction of particle pairs separated by a distance r in the scattering volume. The scattering volume viewed by the photodetector is assumed to be quasi one dimensional, with its length l being much larger than the beam radius σ. Equation (2) states that the light scattered by each pair of particles contributes a phase factor $\cos(q\tau\delta v)$ (because of the frequency beating) to the correlation function $G(\tau)$, and $G(\tau)$ is an incoherent sum of these ensemble-averaged phase factors over all the particle pairs in the scattering volume. The weighted average over r is required because the photodetector receives light from particle pairs that have a range of separations ($0 < r \leq l$), and their contributions to the scattered intensity are proportional to $h(r)$. The function $G(\tau)$ yields information about the velocity differences in

T. Narayanan and P. Tong are with the Department of Physics, Oklahoma State University, Stillwater, Oklahoma 74078. The other authors are with the Department of Physics and Astronomy, University of Pittsburgh, Pittsburgh, Pennsylvania 15260.

Received 18 February 1997; revised manuscript received 9 June 1997.

0003-6935/97/307639-06$10.00/0

the direction of $\mathbf{q}$ and at various scales r up to l. With the PCS technique, one measures the velocity differences without introducing an invasive probe. Moreover it is not necessary to invoke Taylor's frozen turbulence assumption[5] to interpret the measurements.

Over the past several years, the present authors and their collaborators have used the PCS technique to explore small-scale turbulence in various flow geometries. We have studied turbulent flows behind a grid,[4,6,7] in a pipe,[8,9] between two concentric cylinders in which the inner cylinder rotates,[10,11] in a thermal convection cell,[12] and on thin soap films.[13] These studies found notable features of small-scale turbulence and demonstrated that the PCS technique is indeed a powerful tool for the study of the scaling properties of $\delta\mathbf{v}(r)$. In these experiments, the length l of the scattering volume viewed by the photodetector was varied by the changing of the width S of a slit in the collecting optics. Because of the limitations on the collecting optics, the range of l that could be varied in the experiment was only approximately 1 decade (typically from 0.15 to 1.0 mm). The lower cutoff for l is controlled by the beam radius σ. In deriving Eq. (2) we have assumed that the length l is much larger than the beam radius σ, so that the integration over the beam radius can be neglected. When l becomes smaller than σ, the decay of $g(\tau)$ is dominated by the velocity difference over σ rather than over l, and therefore Eq. (2) is no longer valid. In our previous experiments, the slit width S was kept at least 3 times larger than σ. The upper cutoff for l is determined by the coherence distance (or coherence area) at the detecting surface of the photodetector, over which the scattered electric fields are strongly correlated in space.[3] When the slit width S becomes too large, the photodetector sees many temporally fluctuating speckles (or coherence areas), and consequently fluctuations of the scattered intensity $I(t)$ will be averaged out over a range of q values ($= q_0 \pm \Delta q$) spanned by the detecting area. For spatially uncorrelated particle motions, such as Brownian diffusion, this spatial averaging over Δq affects only the signal-to-noise ratio of the measured $g(\tau)$ but the decay rate of $g(\tau)$ remains unchanged.[3] In turbulent and other self-similar flows, however, particle motions at different points are strongly correlated and the spatial averaging effect changes both the signal-to-noise ratio and the functional form of $g(\tau)$. This effect has been studied both theoretically and experimentally by Måløy *et al.*[14]

In this paper we present a new collecting optics for the PCS method with which one can increase the upper cutoff length for l and measure the velocity difference $\delta\mathbf{v}(r)$ over a wider range of r. In studies of turbulent flows, it is always desirable to expand the length scale range so that the scaling laws of $\delta\mathbf{v}(r)$ over varying r can be tested with high accuracy.[15] We present experimental details in Section 2 and discuss the results in Section 3. Finally, the work is summarized in Section 4.

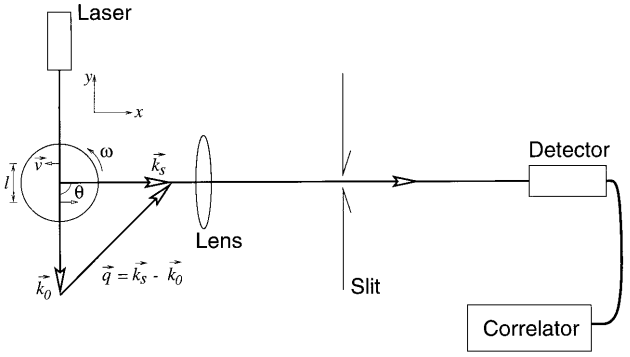

Fig. 1. Schematic diagram of the experimental setup and the scattering geometry.

2. Experiment

To test the new optical arrangement for the PCS technique, we used a turntable to generate rigid body rotation. Figure 1 shows the experimental setup and the scattering geometry. The sample cell was a cylindrical cuvette having an outer diameter of 2.73 cm and a height of ~5 cm. It was filled with 1,2-propylene glycol whose refractive index $n = 1.434$ and shear viscosity $\eta = 40.4$ mPa s (at 25 °C). This viscosity is more than 40 times larger than that of water. A small amount of polystyrene latex spheres of 0.1-μm diameter was seeded in 1,2-propylene glycol with a volume fraction $\phi \simeq 1.5 \times 10^{-4}$. The filled cuvette was mounted coaxially on the turntable, and the axle of the table was coupled to a geared motor that produces smooth rotation. We generated controlled rotation by turning the table at a slow but uniform angular velocity $\omega = 2.5$ rad/s. Because the densities of 1,2-propylene glycol ($= 1.036$ g/cm^3) and the polystyrene particles ($= 1.05$ g/cm^3) are closely matched, the particles faithfully follow the motion of the fluid. Because of the high viscosity of 1,2-propylene glycol, the whole fluid sample was practically under a rigid body rotation and the Brownian motion of the particles was negligible. As a result, fluctuations of the scattered light intensity were dominantly produced by the rotational motion of the particles. In this case, an analytic form for $G(\tau)$ can be obtained. It can be shown from Fig. 1 that the beating frequency $\mathbf{q} \cdot \delta\mathbf{v}(r) = (\mathbf{k}_s - \mathbf{k}_0) \cdot (\omega r\hat{\mathbf{x}}) = k_s\omega(\sin\theta)r$, where $k_s = k_0 = 2\pi n/\lambda$. The function $G(\tau)$ in Eq. (2) then becomes

$$G(\tau) = \int_0^l \mathrm{d}r h(r)\cos[k_s\omega(\sin\theta)r\tau] = \left[\frac{\sin(\Gamma\tau)}{\Gamma\tau}\right]^2, \quad (3)$$

where

$$\Gamma = k_s\omega(\sin\theta)l/2. \quad (4)$$

In obtaining Eq. (3) we have omitted the integral over δv in Eq. (2) because δv is no longer a random variable for rigid body rotation. As mentioned in Section 1, the length l of the scattering volume has been assumed to be much larger than the beam radius σ, so that the integration over σ can be neglected. In fact,

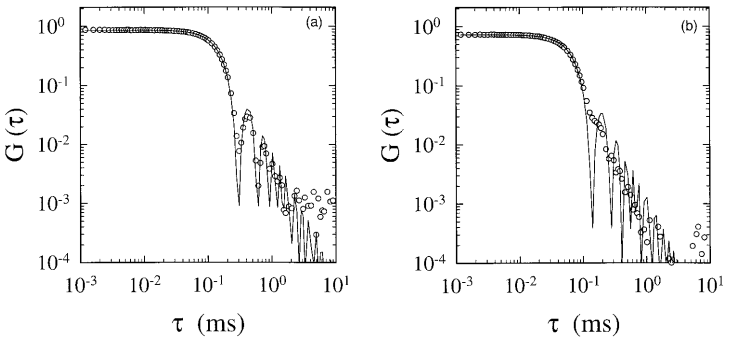

Fig. 2. Measured $G(\tau)$ as a function of the delay time τ. The experimental conditions are (a) $S = 0.35$ mm, $M = 0.45$, (b) $S = 1.25$ mm, $M = 0.65$. The solid curve in (a) is a fit by Eq. (3) with $b = 0.858$ and $\Gamma = 10.57$ $(\text{ms})^{-1}$. The solid curve in (b) is a plot of Eq. (3) with $b = 0.723$ and $\Gamma = 22.84$ $(\text{ms})^{-1}$.

for rigid body rotation the integration over σ is not needed because the velocity gradient in the transverse direction of the beam is zero (assuming that the laser beam is shone through the rotation center).

Figure 1 shows the conventional light-scattering setup that was used first in the experiment. The incident beam from an argon-ion laser with a typical operating power of $\sim$1 W and $\lambda = 514.5$ nm was directed to and focused at the center of the sample cell by a planoconvex lens. The laser beam in the fluid was then projected onto a variable slit by another planoconvex lens. The width S of the slit could be varied from 0 to 5 mm in steps of 0.01 mm. A photomultiplier tube placed at a distance of $\sim$1.3 m behind the slit was used to record the scattered light intensity $I(t)$ passing through the slit. The entire collecting optics was mounted on a rotating arm, such that the scattered intensity could be measured at different scattering angles θ (from 10° to 120°). Most of the measurements described below were conducted at $\theta = 90°$. The digital signal from the photomultiplier was fed to an ALV-5000 multiple-tau correlator, which calculates the correlation function $g(\tau)$ in real time. With the collecting optics shown in Fig. 1, the length l of the scattering volume viewed by the photomultiplier is given by $l = S/(M \sin\theta)$, where the magnification factor M is defined as the ratio of the image distance to the object distance. Note that one can vary l by changing either M or S. In the previous light-scattering studies of turbulent flows,[4,6–10] $g(\tau)$ was measured as a function of S while M was kept at a fixed value ($M \simeq 1$). Our aims in this experiment are to study the effect of changing M and S on the measured $g(\tau)$ and to optimize the collecting optics in order to expand the range of r, over which $\delta\mathbf{v}(r)$ is measured.

3. Results and Discussion

A representative $G(\tau)$ [$= g(\tau) - 1$] measured at $\omega = 2.5$ rad/s, $S = 0.35$ mm, $M = 0.45$, and $\theta = 90°$ is displayed in Fig. 2(a). To show the small oscillations in $G(\tau)$ more clearly, we plot the measured $G(\tau)$ on a log–log scale. The solid curve represents a fit of Eq. (3) to the data with $b = 0.858$ and $\Gamma = 10.57$ $(\text{ms})^{-1}$. It is seen that Eq. (3) fits the data well all the way down to the noise level at $G(\tau) \simeq 10^{-3}$. It is found that the measured $G(\tau)$ starts to change its functional form when the slit width S exceeds 0.55 mm, while all the other experimental parameters are kept the same. Figure 2(b) shows the measured $G(\tau)$ at $\omega = 2.5$ rad/s, $S = 1.25$ mm, and $M = 0.65$. The solid curve in Fig. 2(b) is a plot of Eq. (3) with $b = 0.723$ and $\Gamma = 22.84$ $(\text{ms})^{-1}$. While the main decay portion of $G(\tau)$ can still be fitted by Eq. (3), the oscillations in Eq. (3) are no longer visible in the measured $G(\tau)$. Note that when S is increased, the prefactor b decreases whereas the decay rate Γ increases.

As mentioned in Section 1, when the slit is opened up the photomultiplier receives the scattered light with a range of q values ($= q_0 \pm \Delta q$), and the oscillations in the measured $G(\tau)$ are averaged out by different values of Δq spanned by the detecting area. It has been assumed in Eq. (3) that all the scattered light has the same q value. To include the effect of the spatial averaging over Δq, Eq. (3) needs to be rewritten as[14]

$$G(\tau) = \int_0^l \mathrm{d}r h(r) f^2(Mr/r_c) \cos[k_s \omega(\sin\theta) r\tau], \quad (5)$$

where $f(Mr/r_c)$ describes the spatial correlation of the scattered electric fields at the detecting surface for a given extended light source of size Mr. In our experiment, Mr is the length variable projected on the slit. For the collecting optics shown in Fig. 1, the photodetector has a circular detecting area πa^2 and is placed at a distance R behind the slit. In this case, the coherence length $r_c = R/(k_0 a)$ and the correlation function $f(x) = J_1(x)/x$ with $J_1(x)$, being the first-order Bessel function.[14]

The spatial averaging over Δq not only averages out the oscillations in $G(\tau)$ but also affects the l dependence of the decay rate $\Gamma(l)$. The triangles in Fig. 3 show the measured Γ for different values of l. The value of Γ was obtained by fitting Eq. (3) to the main decay portion of the measured $G(\tau)$ (see Fig. 2). In the measurements, M was fixed at 0.148 and S was varied from 0.15 to 1.25 mm. It is seen that the measured $\Gamma(l)$ first increases linearly with l up to a value $l_c \simeq 3.7$ mm and then it levels off. According to Eq. (4), the decay rate $\Gamma(l)$ [which is proportional to the maximum velocity difference $\delta v(l)$] should be a linear function of l, as $\Gamma(l) \simeq \mathbf{q} \cdot \delta\mathbf{v}(l) \sim k_s \omega l$ for rigid body rotation. Figure 3 reveals that the measured $\Gamma(l)$ shows the expected l dependence only when S is

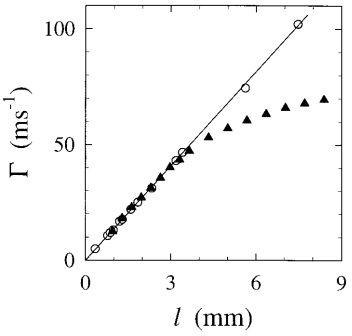

Fig. 3. Measured Γ for different values of l. The triangles were obtained when M was fixed at 0.148 and S was varied from 0.15 to 1.25 mm. The circles were obtained when S was fixed at 0.35 mm and M was varied form 0.047 to 1.03. The solid line is a linear fit to the circles.

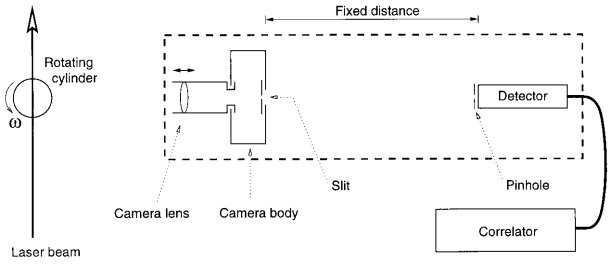

Fig. 4. Schematic diagram of the new optical arrangement for the measurement of $g(\tau)$.

kept at a value smaller than the cutoff width $S_c \equiv l_c M \simeq 0.55$ mm. This value of S_c is found to be independent of the magnification factor M. It is also found that the measured $G(\tau)$ maintains the characteristic oscillations shown in Fig. 2(a) for all values of M so long as $S \leq S_c$. This behavior of the measured $\Gamma(l)$ suggests that the leveling-off effect shown in Fig. 3 is indeed caused by the spatial averaging over Δq. Clearly the departure of the measured $\Gamma(l)$ from the linear behavior at large l demarcates the failure of using $G(\tau)$ to obtain information about the maximum velocity difference $\delta\mathbf{v}(l)$. Figure 3 thus suggests that to accurately measure $\delta\mathbf{v}(l)$, one needs to keep the slit width $S \leq S_c$. Put in another way, to avoid the spatial averaging over Δq the correlation function $f(Mr/r_c)$ in Eq. (5) should be kept at a value larger than $f(S_c/r_c) = J_1(1.45)/1.45 \simeq e^{-1}$. Here we calculate $r_c = R/(k_0 a) = 0.38$ mm by using the experimental parameters $R = 1300$ mm, $a = 0.195$ mm, and $k_0 = 1.75 \times 10^4$ mm^{-1}.

From the above measurements we find that the range of the slit width, over which $\delta\mathbf{v}(l)$ can be accurately measured, is rather limited (0.15 mm $\leq S \leq$ 0.55 mm for our setup). This range could be widened by an increase in the distance R between the photomultiplier tube and the slit (i.e., an increase in r_c). However, increasing R by a factor of 10 will result in a drastic reduction in the scattering intensity because the intensity goes as $1/R^2$. An alternative way to increase the useful range of l is to vary M while keeping S constant ($\leq S_c$). The circles in Fig. 3 show the measured $\Gamma(l)$ obtained when S was fixed at 0.35 mm and M was varied from 0.047 to 1.03. It is seen that over the whole range of l, the measured Γ exhibits the expected linear behavior in l. The solid line in Fig. 3 is a linear fit to the circles. The fitted line passes through the origin, indicating that the velocity difference $\delta\mathbf{v}(l)$ vanishes as l goes to 0. According to Eq. (4), the decay rate $\Gamma = k_s \omega(\sin\theta) l/2 = 21.9l$ (ms^{-1}). The slope of the fitted line in Fig. 3 is $\Gamma/l = 13.63$ (mm ms)$^{-1}$, which is only 62.2% of the calculated value. In Fig. 3 the length l of the scattering volume is computed without including the magnification by the cylindrical sample cell itself. Taking this effect into account, we have $\Gamma/l = 13.63n = 19.6$ (mm ms)$^{-1}$, which is close to, but still 10.5% smaller than, the calculated value. One source for the small deviation is the experimental uncertainties for the calibration of the length l (and hence Γ/l). We estimate that the errors for l were ±8%. Another possibility is that, in Fig. 3, Γ was obtained with an approximate (but analytic) expression for $G(\tau)$ [i.e., Eq. (3)] rather than the exact (but nonanalytic) solution of Eq. (5). Because $f(Mr/r_c)$ in Eq. (5) gives extra weights to the particle pairs with small separations, the decay rate Γ obtained with $f(Mr/r_c)$ could be larger than that without $f(Mr/r_c)$. To verify this argument, we numerically integrate Eq. (5) and find that the fitted Γ without $f(Mr/r_c)$ is ~3% smaller than that with $f(Mr/r_c)$.[16] To verify Eq. (4) further, we changed the rotation speed ω and find that Γ is indeed proportional to ω. We also measured Γ at different scattering angles θ (from 10° to 120°) and the obtained Γ is found to be independent of θ. Because the length l changes with θ by means of $l = l_0/\sin\theta$ ($l = l_0$ at $\theta = 90°$), the sin θ dependence in Γ is canceled out and hence Γ becomes independent of θ.

In the measurements discussed above, M could be varied between 0.045 and 1. For $M = 1$, one could also change the slit width S from 0.15 to 0.55 mm. With the combined changes of S and M, we were able to vary l by approximately 2 decades (0.15 mm $\leq l \leq$ 12.22 mm). To facilitate the changes in M, we used 13 planoconvex lenses of different focal lengths ranging from 1.9 to 11 cm. For each measurement with different M, we had to change the lens and readjust its position while keeping the other components in the collecting optics unchanged. Because the center of the lens has to be placed exactly on the optical axis of the entire collecting optics, realignment of the lens each time when it is changed becomes tedious and cumbersome. This is especially true when many lenses are needed in order to vary l by 2 orders of magnitude. Because spherical aberrations can alter the actual length l viewed by the photomultiplier [and hence the decay rate of the measured $G(\tau)$], high-quality lenses are needed when the value of M becomes small.

To overcome these experimental difficulties, we redesigned the collecting optics. Figure 4 shows a schematic diagram of the new optical arrangement.

Having realized that camera lenses are usually of high quality (with minimal aberrations) and that the precision of camera mountings makes the optical alignment almost automatic, we replaced the single-lens optics shown in Fig. 1 with a single-lens reflex camera body together with three Nikon lenses: a 105-mm microlens, a 50-mm standard lens, and a 35-mm wide-angle lens. A slit of fixed width $S = 0.4$ mm ($<S_c$) was installed on the film (image) plane of the camera body. The camera lens projected the scattered laser beam of length l right on the slit. The three Nikon lenses were used, respectively, to vary M and hence l. A photodetector was mounted behind the slit on an x–y translation stage (not shown in Fig. 4) to facilitate the optical alignment. Also not shown is a light shield that ran from the back of the camera to the photodetector. The camera and the photodetector were mounted together on a solid arm, and their relative positions were fixed so that they acted like a single compact piece of apparatus. The operating procedure for this setup was quite straightforward. Using the viewfinder on the camera, we adjusted the position of the lens so that the scattering volume was in sharp focus. The value of M was noted. The shutter of the camera was then opened and the correlation measurements were carried out. The value of M for a given setup can be estimated by the ratio of the known focal length of the lens used to the object distance shown on the focusing dial on the camera. Alternatively, one can take a photograph of a meter stick placed at the sample position and find the value of M from the ratio of the length appearing on the film to its actual length shown on the meter stick. With the above optical arrangement, M can be varied from 1.0 to 0.033. If an additional photographic bellows extender is mounted in between the lens and the camera body, we expect that the largest value of M can be extended to $\sim$4. This will expand the variable range of M to 2 decades.

With the new optical arrangement, one needs to align the photodetector with respect to the slit (in the camera body) only once. The alignment of the lens to the slit is automatic. Most of the delicate optical alignments associated with the conventional setup shown in Fig. 1 are no longer necessary and a wide range of l can be obtained. Because S is fixed at a constant value smaller than S_c, the function $f(Mr/r_c)$ in Eq. (5) becomes independent of M. Furthermore, the prefactor b in Eq. (1) (which is a measure of the signal-to-noise ratio) remains constant. These new features are particularly useful for the study of turbulent and other self-similar flows. When $f(Mr/r_c)$ in Eq. (5) becomes independent of M, the correlation function $G(\tau)$ will have a scaling form $G(\Gamma\tau)$ with $\Gamma \simeq \mathbf{q} \cdot \delta\mathbf{v}(l)$. In the case of rigid body rotation, we have $\Gamma\tau \sim \tau/M$ [see Eq. (4)]. Indeed, the measured $G(\tau)$ with the new optical setup is found to be of the scaling form $G(\tau/\mathrm{M})$. Log–log plots of $G(\tau)$ for different values of M can be brought into coincidence with the scaling variable τ/M. Figure 5 shows the measured $G(\tau)$ as a function of τ/M for five different values of M. It is seen that the collapsing of the curves is excellent.

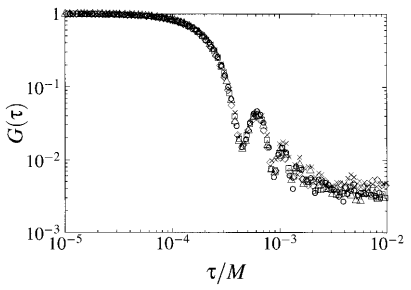

Fig. 5. Measured $G(\tau)$ as a function of τ/M for different values of M. New collecting optics was used in the measurements, and the values of M are 0.50 (◇), 0.33 (□), 0.20 (△), 0.14 (○), and 0.083 (×).

Figure 5 thus demonstrates that our new optical arrangement can provide full spatial coherence for the measurement of $g(\tau)$.

4. Conclusion

We have used homodyne photon correlation spectroscopy to measure the velocity difference $\delta\mathbf{v}(l)$ separated by a distance l. With the conventional light-scattering setup, one can vary l by changing either the width S of a slit in the collecting optics or the magnification factor M of the scattered laser beam projected on the slit. In the present experiment, we studied the effect of changing S and M on the intensity autocorrelation function $g(\tau)$. The measured $g(\tau)$ is found to be of scaling form for different values of M, provided that S is kept at a value below the critical width S_c. A new convenient collecting optics is devised to expand the variable range of l up to 2 decades, over which $\delta\mathbf{v}(l)$ can be accurately measured. The new scheme is useful for the study of turbulent and other self-similar flows, in which one is interested in testing the scaling laws of $\delta\mathbf{v}(l)$ over varying l.

We thank C. K. Chan for useful discussions. This research was supported by the National Aeronautics and Space Administration under joint grant NAG3-1613. In addition, P. Tong was supported in part by the U.S. National Science Foundation under grant DMR-9623612, and W. Goldburg was supported in part by the U.S. National Science Foundation under grant DMR-8914351 and also by an award from the BP Corporation.

References

1. P. J. Bourke, J. Butterworth, L. E. Drain, P. A. Egelstaff, A. J. Hughes, P. Hutchinson, D. A. Jackson, E. Jakeman, B. Moss, J. O'Shaughnessy, E. R. Pike, and P. Schofield, "A study of the spatial structure of turbulent flow by intensity-fluctuation spectroscopy," J. Phys. A **3,** 216–228 (1970).
2. G. G. Fuller, J. M. Rallison, R. L. Schmidt, and L. G. Leal, "The measurement of velocity gradients in a laminar flow by homodyne light-scattering spectroscopy," J. Fluid Mech. **100,** 555–575 (1980).
3. B. J. Berne and R. Pecora, *Dynamic Light Scattering* (Wiley, New York, 1976), p. 40.
4. P. Tong, W. I. Goldburg, C. K. Chan, and A. Sirivat, "Turbulent transition by photon correlation spectroscopy," Phys. Rev. A **37,** 2125–2133 (1988).

5. G. I. Taylor, "The spectrum of turbulence," Proc. R. Soc. London A **164,** 476–490 (1938).
6. P. Tong and W. I. Goldburg, "Experimental study of relative velocity fluctuations in turbulence," Phys. Lett. A **127,** 147–150 (1988).
7. H. K. Pak, W. I. Goldburg, and A. Sirivat, "Measuring the probability distribution of the relative velocities in grid-generated turbulence," Phys. Rev. Lett. **68,** 938–941 (1992); "An experimental study of weak turbulence," Fluid Dyn. Res. **8,** 19–31 (1991).
8. P. Tong and W. I. Goldburg, "Relative velocity fluctuations in turbulent flows at moderate Reynolds number I. Experimental," Phys. Fluids **31,** 2841–2848 (1988).
9. W. I. Goldburg, P. Tong, and H. K. Pak, "A light scattering study of turbulence," Physica D **38,** 134–140 (1989).
10. P. Tong, W. I. Goldburg, and J. S. Huang, "Measured scaling properties of inhomogeneous turbulent flows," Phys. Rev. A **45,** 7222–7230 (1992).
11. K. J. Måløy and W. I. Goldburg, "Spatial anisotropy of velocity fluctuations on small length scales in a Taylor–Couette cell," Phys. Rev. E **48,** 322–327 (1993); "Measurements on transition to turbulence in a Taylor–Couette cell with oscillatory inner cylinder," Phys. Fluids A **5,** 1438–1442 (1993).
12. P. Tong and Y. Shen, "Relative velocity fluctuations in turbulent Rayleigh–Bénard convection," Phys. Rev. Lett. **69,** 2066–2069 (1992).
13. H. Kellay, X.-l. Wu, and W. I. Goldburg, "Experiments with turbulent soap films," Phys. Rev. Lett. **74,** 3975–3978 (1995).
14. K. J. Måløy, W. I. Goldburg, and H. K. Pak, "Spatial coherence of homodyne light scattering from particles in a convective field," Phys. Rev. A **46,** 3288–3291 (1992).
15. See, e.g., P. Tong and W. I. Goldburg, "Relative velocity fluctuations in turbulent flows at moderate Reynolds number II. Model calculation," Phys. Fluids **31,** 3253–3259 (1988).
16. C. Cheung, "A study of the surface motion on a turbulent fluid," Ph.D. dissertation (University of Pittsburgh, Pittsburgh, Pa., 1997).